Monthly Notices of the ROYAL ASTRONOMICAL SOCIETY

Mon. Not. R. Astron. Soc. **400,** 90–99 (2009) doi:10.1111/j.1365-2966.2009.15443.x

Constraining the energy budget of GRB 080721

R. L. C. Starling,[1★] E. Rol,[1,2] A. J. van der Horst,[3] S.-C. Yoon,[4] V. Pal'shin,[5] C. Ledoux,[6] K. L. Page,[1] J. P. U. Fynbo,[7] K. Wiersema,[1] N. R. Tanvir,[1] P. Jakobsson,[8] C. Guidorzi,[9,10] P. A. Curran,[11] A. J. Levan,[12] P. T. O'Brien,[1] J. P. Osborne,[1] D. Svinkin,[5] A. de Ugarte Postigo,[6] T. Oosting[13] and I. D. Howarth[14]

[1]*Department of Physics and Astronomy, University of Leicester, University Road, Leicester LE1 7RH*
[2]*Astronomical Institute, University of Amsterdam, PO Box 94249, 1090 GE, Amsterdam, the Netherlands*
[3]*NASA Postdoctoral Program Fellow, NSSTC, 320 Sparkman Drive, Huntsville, AL 35805, USA*
[4]*UCO/Lick Observatory, Department of Astronomy and Astrophysics, University of California, Santa Cruz, CA 95064, USA*
[5]*Ioffe Physico-Technical Institute, Laboratory for Experimental Astrophysics, 26 Polytekhnicheskaya, St Petersburg 194021, Russia*
[6]*European Southern Observatory, Alonso de Córdova 3107, Casilla 19001, Vitacura, Santiago, Chile*
[7]*Dark Cosmology Centre, Niels Bohr Institute, University of Copenhagen, Juliane Maries Vej 30, DK-2100 Copenhagen Ø, Denmark*
[8]*Centre for Astrophysics and Cosmology, Science Institute, University of Iceland, Dunhagi 5, 107 Reykjavík, Iceland*
[9]*INAF – Osservatorio Astronomico di Brera, Via E. Bianchi 46, I-23807 Merate (LC), Italy*
[10]*Physics Department, University of Ferrara, via Saragat 1, 44100 Ferrara, Italy*
[11]*Mullard Space Science Laboratory, University College London, Holmbury St. Mary, Dorking, Surrey RH5 6NT*
[12]*Department of Physics, University of Warwick, Coventry CV4 7AL*
[13]*Department of Astrophysics, University of Nijmegen, PO Box 9010, 6500 GL, Nijmegen, the Netherlands*
[14]*Department of Physics and Astronomy, University College London, Gower Street, London WC1E 6BT*

Accepted 2009 July 22. Received 2009 July 20; in original form 2008 December 11

ABSTRACT

We follow the bright, highly energetic afterglow of *Swift*-discovered GRB 080721 at $z = 2.591$ out to 36 d or 3×10^6 s since the trigger in the optical and X-ray bands. We do not detect a break in the late-time light curve inferring a limit on the opening angle of $\theta_j \geq 7\overset{\circ}{.}3$ and setting tight constraints on the total energy budget of the burst of $E_\gamma \geq 9.9 \times 10^{51}$ erg within the fireball model. To obey the fireball model closure relations, the gamma-ray burst (GRB) jet must be expanding into a homogeneous surrounding medium and likely lies behind a significant column of dust. The energy constraint we derive can be used as an observational input for models of the progenitors of long GRBs: we discuss how such high collimation-corrected energies could be accommodated with certain parameters of the standard massive star core-collapse models. We can, however, most probably rule out a magnetar progenitor for this GRB which would require 100 per cent efficiency to reach the observed total energy.

Key words: gamma-rays: bursts.

1 INTRODUCTION

The discovery (Costa et al. 1997; van Paradijs et al. 1997) of afterglows to long-duration gamma-ray bursts (GRBs) showed that they occurred in star-forming galaxies at high redshifts. Many aspects of the observed GRB behaviour could be explained reasonably well by the relativistic fireball models, in which the prompt emission is largely produced by shocks internal to the outflow and the long-lived afterglow by the outflow impacting and shocking the external ambient medium (Mészáros & Rees 1997; Sari et al. 1998). However, it was early appreciated that if they emitted isotropically then the radiative energies implied for some bursts would be very large (e.g. in excess of a solar rest mass in the case of GRB 990123; Kulkarni et al. 1999). Since no known mechanism can produce high-energy photons with efficiency approaching 100 per cent, the total explosive energy required would be even greater, implausibly large for a stellar core-collapse powered event.

The energetics argument led to the expectation that the GRB outflow must be confined to a jet, reducing the overall energy requirements. In that case, a sufficiently massive core collapsing to a black hole might produce an outflow which could pierce a hydrogen-stripped envelope to still produce a relativistic jet (MacFadyen & Woosley 1999). This picture received support from the observation of concurrent supernova events at GRB sites for some (low-redshift) low-luminosity bursts (Galama et al. 1998;

★E-mail: rlcs1@star.le.ac.uk

© 2009 The Authors. Journal compilation © 2009 RAS

Hjorth et al. 2003; Stanek et al. 2003; Pian et al. 2006). The class of GRB-supernovae could be explained by the explosion of a Wolf–Rayet star, and it has been widely assumed that this progenitor must account for most if not all long GRBs.

A strong prediction of all collimated models is that the observed light curve should exhibit an achromatic break, visible in both optical and X-ray light curves, when the relativistic outflow slows to the point that the Doppler beaming angle becomes wider than the opening angle of the jet (Rhoads 1997): the later the break time, the wider the jet. In the pre-*Swift,* era a number of bursts with good afterglow observations showed breaks in the optical, at times ranging from a few hours to a few days. Furthermore, it was contended that the implied jet opening angles anticorrelated with the isotropic-equivalent gamma-ray energies $E_{\rm iso}$ (Frail et al. 2001) – in other words, corrected for collimation nearly all bursts seemed to be accessing a rather standard energy reservoir (to within about an order of magnitude), potentially usable as standard candles at high redshift. While the total rotational energies available from a collapsing core may be of the order of 10^{54} erg, the maximal extraction of energy is unlikely to exceed 10^{51}–10^{52} erg (Paczynski 1998; Popham, Woosley & Fryer 1999). With this in mind, the standard energy reservoir with energies of $\sim 10^{51}$ erg appeared very attractive.

Unfortunately, the X-ray data available pre-*Swift* only provided definitive evidence of (single) breaks for a few bursts. One of the expectations of *Swift* was that many more bursts would be seen with clear breaks in the X-ray coincident with optical breaks. After more than four years of operations, this is not what has been found. In fact, the situation is much more confusing, with X-ray light curves exhibiting complex behaviour including flares and plateaux (Nousek et al. 2006; O'Brien et al. 2006; Willingale et al. 2007). When late breaks (beyond a few hours) are seen they rarely coincide in time or degree with optical breaks, and are hard to reconcile with simple fireball model predictions (e.g. Panaitescu et al. 2006), though there are notable exceptions. It is possible that from X-ray data alone a number of jet breaks, particularly those at late times or those which turn over rather smoothly, may go undetected through misinterpretation of their light curves. These so-called hidden breaks may be revealed on comparison of X-ray light curves with optical light curves (Curran, van der Horst & Wijers 2007), but the emphasis remains on X-ray light curves for break detection owing to the large numbers of well-sampled X-ray light curves now available.

Most crucially, in many GRBs no temporal break is seen at all to late times, implying much more energy than expected. The most extreme example to date is that of GRB 060729, which continued a smooth X-ray power-law decline for 125 d, implying an opening angle greater than 28° (Grupe et al. 2007). This source continues to be monitored in the X-rays with *Chandra* and was still detected one year after the GRB event (Grupe et al. 2007). The light curve now shows a possible break at ∼290 d: the nature of this break is not yet known. While the modest luminosity and low redshift of GRB 060729 ($E_{\rm iso} \sim 7 \times 10^{51}$ erg; Grupe et al. 2007) make it unsuitable to test collapsar models to their limits, such observations provide a crucial guide to further theoretical developments. If such high collimation-corrected energies continue to be inferred, then the situation looks bleak for simple core-collapse models as the explanation for the high-luminosity long GRBs. In fact, it would suggest that a different progenitor is required for high- and low-luminosity long bursts. On the other hand, if late breaks are seen, although the jet model is not proven this could provide evidence for an upper envelope to the energy tapped by GRBs which may still be consistent with that available in principle from core collapse, but would require a new understanding of how such high efficiencies of radiative emission could be achieved.

In this paper, we follow a high-redshift GRB with a high isotropic energy out to late times to search for a jet break and thereby measure the total energy budget of the prompt gamma-ray emission. In Section 2, we describe the gamma-ray, X-ray and optical observations and analyses. We derive the GRB fluence in Section 3. In Section 4 we characterize the afterglow spectra and light curves and in Section 5 we compare the results to the fireball model discussing the possibility of an early jet break. In Section 6, we calculate limits on the jet opening angle and collimation-corrected energy of this GRB. In Section 7, we note the caveats associated with our results, discuss the energetics of this GRB in relation to current popular progenitor models and compare this GRB to other bursts of interest. In Section 8 we conclude.

2 OBSERVATIONS

Throughout this paper, we use the conventions $F \propto \nu^{-\beta} t^{-\alpha}$ for temporal and spectral power-law models. Errors are quoted at the 90 per cent confidence level unless otherwise stated.

2.1 Gamma ray

The *Swift* satellite triggered on GRB 080721 on 2008 July 21 at 10:25:16.979 UT ($T_{0,\rm BAT}$). The Burst Alert Telescope (BAT) gamma-ray light curve showed approximately six peaks, three strong followed by three weak, spanning $T_{0,\rm BAT} - 11$ s to $T_{0,\rm BAT} + 370$ s and the burst duration as defined by the T_{90} parameter was 16.2 ± 4.5 s (Marshall et al. 2008). The BAT data were reduced using the *Swift* analysis software version 29 (released 2008 June 29, part of HEASOFT 6.5.1).

The *Konus-Wind* experiment triggered the prompt emission of GRB 080721 beginning at 10:25:10.927 UT ($T_{0,\rm KW}$). The propagation delay from *Swift* to *Konus-Wind* is 3.375 s for this GRB, that is by correcting for this factor one sees that the *Konus-Wind* trigger time corresponds to $T_{0,\rm BAT} - 9.427$ s. From $T_{0,\rm KW}$ to $T_{0,\rm KW} + 482.560$ s, 64 spectra in 101 channels (from 20 keV to 15 MeV) were accumulated on time-scales varying from 64 ms near the trigger time to 8.192 s by the time the signal became undetectable (Golenetskii et al. 2008). Data were processed using standard *Konus-Wind* analysis tools. The 20 keV–7 MeV peak flux is $(2.11 \pm 0.35) \times 10^{-5}$ erg cm^{-2} s^{-1} (using the spectrum accumulated over the main peak, from $T_{0,\rm KW} + 8.448$ s to $T_{0,\rm KW} + 10.494$ s). The corresponding isotropic peak luminosity is $L_{\rm iso,max} = (1.11 \pm 0.18) \times 10^{54}$ erg s^{-1}.

The gamma-ray light curves from both BAT and *Konus-Wind* are shown in Fig. 1.

2.2 X-ray

The *Swift* X-Ray Telescope (XRT) slewed to the burst and began observations in a Windowed Timing (WT) mode 113 s after the BAT trigger, detecting the tail of the prompt emission and the X-ray afterglow, and transitioned to the Photon Counting (PC) mode in the second orbit of data collection. With XRT we have monitored the bright afterglow out to 1.4×10^6 s or 16 d (Marshall et al. 2008). The XRT data were reduced using the *Swift* analysis software version 29, as described in Evans et al. (2007, 2009). Light curves use dynamic binning with a minimum binsize of 5 s and spectra are grouped such that a minimum of 20 counts lie in each bin.

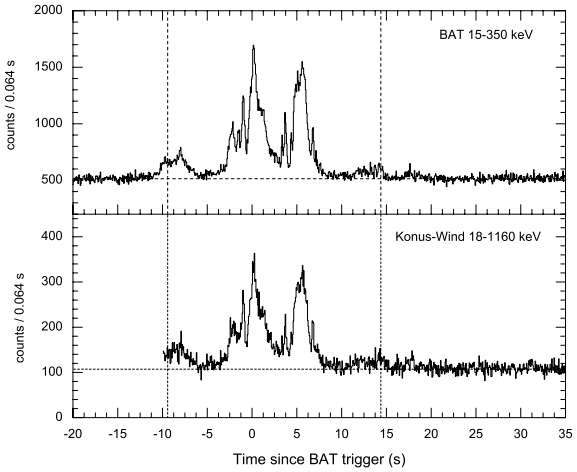

Figure 1. *Swift* BAT (top panel) and *Konus-Wind* (lower panel) 64 ms light curves of the prompt emission. The dashed vertical lines indicate the time interval adopted for joint spectral fits.

We triggered our target-of-opportunity programme on the *XMM–Newton* satellite to obtain continued observations of GRB 080721 once the X-ray afterglow flux had fallen below the sensitivity limits of the *Swift* XRT. The afterglow is clearly detected with the European Photon Imaging Cameras' (EPIC) pn in a 12 ks observation performed on 2008 August 12 and again in a 73 ks observation beginning 2008 August 26 and ending 2008 August 27. The *XMM–Newton* data were reduced using the standard *XMM–Newton* Science Analysis Software version 20080701-1801. The second observation is partially affected by high background so we removed periods of background with >1 count s^{-1} in the PN data leaving 46.5 ks of useful exposure time. We used the tool EDETECT-CHAIN to identify the source position and measure a background-subtracted count rate. We then used ESPECGET to create spectra and obtain the flux at each epoch by assuming a spectral shape identical to that of the best fit to the time-averaged *Swift* XRT PC mode spectrum.

2.3 Optical

The Ultraviolet-Optical Telescope (UVOT) on-board *Swift* began observations 118 s after the BAT trigger and found a bright optical afterglow in all optical filters, while the source was not detected in the UV filters (Marshall et al. 2008). Here we will focus on the *white* and v bands where temporal coverage was most comprehensive.

We initiated ground-based observations once GRB 080721 became visible from the Roque de Los Muchachos Observatory, La Palma. Observations were taken using the Nordic Optical Telescope (NOT) and the Liverpool Telescope (LT), followed several hours later by observations from Paranal Observatory with the Very Large Telescope (VLT) UT2 (Kueyen). After the initial observations, we initiated our programme for late-time light-curve monitoring, obtaining further observations with the LT, the Isaac Newton Telescope (INT), the William Herschel Telescope (WHT) and the VLT UT1 (Antu). All optical afterglow photometry is listed in Table 1. Ground-based optical photometry has been reduced in the standard fashion using IRAF (Tody 1986). For the photometric calibration, we used the zero-points for the VLT FORS2, provided by the observatory,[1] after verifying that the corresponding nights were photometric using standard stars. For the r and i filters, we converted the R and I zero-points to the Sloan Digital Sky Survey (SDSS) filters using the conversion at the SDSS webpages.[2] We adopt a Galactic extinction of $E(B-V) = 0.102$ mag (Schlegel, Finkbeiner & Davis 1998).

A low resolution spectrum was taken at the NOT from which we measured a redshift of $z = 2.591 \pm 0.001$ reported in Jakobsson et al. (2008), confirming an earlier redshift determination from independent data (D'Avanzo et al. 2008). Starting on 2008 July 22.121 (0.7 d post-burst), we obtained a sequence of higher resolution spectra using the VLT FOcal Reducer and low dispersion Spectrograph (FORS) 1 in a long-slit spectroscopy mode with a 1.0 arcsec wide slit. The progression of grisms used was 300V (1200 s), 1200B (1800 s) and 600V+GG435 (1800 s). The individual spectra were cosmic ray cleaned using the method of van Dokkum (2001). The seeing stayed relatively stable during the observations, between 1.1 arcsec and 1.3 arcsec, yielding a spectral resolution of 13.4 (300V), 2.9 (1200B) and 5.9 (600V+GG435) Å full width at half-maximum (FWHM). Flux calibration was performed using an observation of the standard star BPM16274. From the optical spectrum, we derive a neutral hydrogen column density of $\log N(\mathrm{H\,I}) = 21.6 \pm 0.10$ cm^{-2}. A more detailed analysis of the optical spectra appears in Fynbo et al. (2009).

3 MEASURING THE GAMMA-RAY BURST FLUENCE

We performed a joint fit to the 20 keV–7 MeV *Konus-Wind* and 15–150 keV BAT spectra, time integrated over the 23.81 s of simultaneous observations (covering the main peaks of gamma-ray emission; Fig. 1). Adopting the Band function model (Band et al. 1993, in which α and β are spectral slopes as opposed to the definitions given in Section 2 used elsewhere in this paper) and allowing for a constant normalization offset between the BAT and *Konus* instruments, we find that the data are well fitted with χ^2/degrees of freedom (d.o.f.) = 105.6/138. We measure a low-energy spectral slope $\alpha = -0.96^{+0.08}_{-0.07}$, high-energy spectral slope $\beta = -2.42^{+0.22}_{-0.38}$ and spectral peak energy $E_{\rm pk} = 497^{+63}_{-61}$ keV. The gamma-ray spectral energy distribution (SED), showing the location of the spectral peak in the *Konus-Wind* energy range at this time, is plotted in Fig. 2. The ratio of BAT to *Konus-Wind* normalization was 0.83 ± 0.04, with all other model parameters being tied. We also split these observations into four time intervals over which we searched for spectral variability. There is no evidence for highly statistically significant ($>3\sigma$) spectral variations within the measured errors; therefore, we use the time-averaged spectral fit parameters in further analysis. We measure a fluence (or time-integrated flux), S, of $(8.81^{+0.77}_{-0.75}) \times 10^{-5}$ erg cm^{-2} (20 keV–7 MeV) from the joint spectral fit.

4 CHARACTERIZING THE AFTERGLOW

4.1 Spectral fits

The X-ray hardness ratio (HR), defined as the count rate ratio in the energy bands 1.5-10 keV/0.3-1.5 keV, indicates that there are no significant X-ray spectral changes throughout the entire duration of *Swift* XRT observations. We have fitted the HR with a constant value and found a value of HR = 0.78 ± 0.01 with χ^2/d.o.f. = 222.36/246. To allow for an increase or decrease in HR, we fitted the data with a linear function and found that this extra d.o.f. does

[1] http://www.eso.org/observing/dfo/quality/FORS2/qc/photcoeff/photcoeffs_fors2.html

[2] http://www.sdss.org/dr6/algorithms/sdssUBVRITransform.html#Lupton2005

Table 1. Overview of optical photometric observations obtained for GRB 080721. The magnitudes are *AB* magnitudes for the *r* and *i* filters. The listed magnitudes are not corrected for Galactic extinction; the listed fluxes are corrected for Galactic extinction. Errors are given at the 1σ level.

$T_{\rm start}$ (UT)	$T_{\rm mid}$ (days since $T_{0,\rm BAT}$)	$T_{\rm exp}$ (s)	Filter	Magnitude	Flux (μJy)	Telescope + Instrument
2008-07-21 10:27:14	0.0019	98.19	White	14.58 ± 0.01	2945 ± 9.000	*Swift* UVOT
2008-07-21 10:37:15	0.0084	9.61	White	16.73 ± 0.07	428 ± 28.0	*Swift* UVOT
2008-07-21 10:39:34	0.0105	98.20	White	16.95 ± 0.03	339 ± 8.00	*Swift* UVOT
2008-07-21 11:51:29	0.0610	196.62	White	19.12 ± 0.11	44.0 ± 4.00	*Swift* UVOT
2008-07-21 12:15:25	0.0777	196.61	White	19.40 ± 0.13	35.0 ± 4.00	*Swift* UVOT
2008-07-22 04:13:23	0.9049	2414.0	White	22.39 ± 0.17	6.00 ± 1.00	*Swift* UVOT
2008-07-24 00:50:14	2.0790	1860.5	White	23.57 ± 0.62	3.00 ± 1.00	*Swift* UVOT
2008-07-21 10:29:01	0.0049	393.4	*v*	14.93 ± 0.01	3876 ± 53.00	*Swift* UVOT
2008-07-21 10:37:54	0.0089	19.4	*v*	16.04 ± 0.13	1404 ± 167.0	*Swift* UVOT
2008-07-21 10:41:20	0.0135	393.5	*v*	16.41 ± 0.04	993 ± 34.0	*Swift* UVOT
2008-07-21 11:58:19	0.0658	196.6	*v*	18.37 ± 0.24	164 ± 36.0	*Swift* UVOT
2008-07-21 12:22:16	0.0820	135.6	*v*	18.13 ± 0.23	204 ± 44.0	*Swift* UVOT
2008-07-21 15:23:23	0.2118	797.2	*v*	19.93 ± 0.47	39.0 ± 17.0	*Swift* UVOT
2008-07-22 04:20:38	0.9074	2524.4	*v*	20.90 ± 0.29	21.0 ± 9.00	*Swift* UVOT
2008-08-01 00:30:33	10.5880	180	*V*	25.57 ± 0.23	0.290 ± 0.061	VLT Antu + FORS2
2008-08-01 00:34:06	10.5905	180	*V*	25.64 ± 0.25	0.272 ± 0.063	VLT Antu + FORS2
2008-07-21 20:51:00	0.4444	980	*R*	20.12 ± 0.12	33.3 ± 3.70	NOT + ALFOSC
2008-07-22 02:36:32	0.6747	30	*R*	20.82 ± 0.08	17.5 ± 1.30	VLT Kueyen + FORS1
2008-07-22 02:41:25	0.6781	30	*R*	20.80 ± 0.12	17.8 ± 2.00	VLT Kueyen + FORS1
2008-07-30 20:57:27	9.4533	2100	*R*	25.22 ± 0.50	0.303 ± 0.140	WHT + API
2008-08-01 00:37:49	10.5931	180	*R*	24.94 ± 0.16	0.393 ± 0.058	VLT Antu + FORS2
2008-08-01 00:41:23	10.5956	180	*R*	25.01 ± 0.17	0.368 ± 0.058	VLT Antu + FORS2
2008-08-10 23:11:45	20.5467	1080	*R*	25.75 ± 0.44	0.186 ± 0.075	VLT Antu + FORS2
2008-08-20 23:40:32	30.5695	2700	*R*	26.47 ± 0.28	0.0960 ± 0.0250	VLT Antu + FORS2
2008-07-21 21:10:12	0.4585	1800	*r*	20.43 ± 0.10	31.7 ± 2.90	LT + RATCAM
2008-07-23 22:40:16	2.5211	1800	*r*	22.86 ± 0.13	3.38 ± 0.400	LT + RATCAM
2008-07-24 21:56:17	3.4959	1500	*r*	23.47 ± 0.12	1.92 ± 0.210	INT + WFC
2008-07-27 21:30:27	6.4759	980	*r*	24.56 ± 0.28	0.705 ± 0.180	INT + WFC
2008-08-01 00:45:06	10.5981	180	*I*	24.16 ± 0.54	0.593 ± 0.290	VLT Antu + FORS2
2008-07-21 22:17:07	0.5050	1800	*i*	20.43 ± 0.22	29.7 ± 6.00	LT + RATCAM

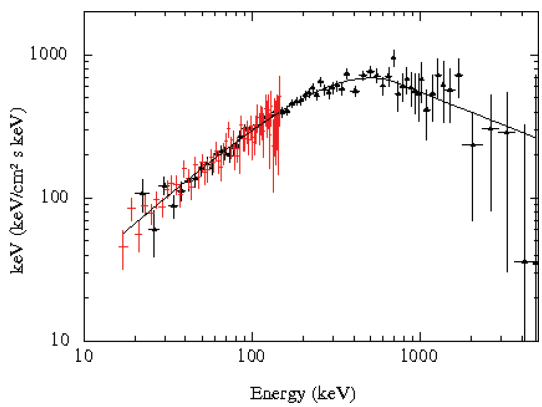

Figure 2. SED (equivalent to a νF_ν representation) showing the 20 keV–7 MeV *Konus-Wind* spectrum (black) and the 15–130 keV BAT spectrum (red, scaled by the BAT-*Konus-Wind* offset) in the time interval $T_{0,\rm BAT} - 16$ s to $T_{0,\rm BAT} + 7.81$ s. The solid line shows the best-fitting Band function, from which the spectral peak energy can be clearly measured at a few hundred keV.

not improve the fit (which then goes to χ^2/d.o.f. = 221.9/245) but is an equally good fit to the constant value assumption.

To investigate spectral evolution further, we created seven time-sliced *Swift* XRT spectra covering almost the entire decay: $T_{0,\rm BAT}$+112–288 s (WT), 304–1376 s (WT), 4.5–7.2 ks (PC orbit 2), 10.3–12.9 ks (PC orbit 3), 16.9–18.7 ks (PC orbit 4), 23.3–92.6 ks (PC from orbit 5–1.16 d) and 137.7–1400 ks (PC from 1.16 d onwards). We fit these spectra simultaneously with an absorbed power law; the Galactic absorption was fixed to $N_{\rm H,gal} = 7 \times 10^{20}$ cm^{-2} (Kalberla et al. 2005), the intrinsic absorption at $z = 2.519$ was tied, that is was required to have the same value at each epoch, and the power-law photon index, $\Gamma = \beta + 1$, and normalization were left as free parameters per epoch. The best fit has χ^2/d.o.f. = 1765/1307 ($\chi^2_{\rm red} = 1.35$). Intrinsic X-ray absorption at the host galaxy is best fitted with $N_{\rm H} = (6.5 \pm 0.5) \times 10^{21}$ cm^{-2}, assuming solar metallicity, and we note that this is comparable to the column density derived in the optical from hydrogen Lyman-α. Plotting the resulting $\beta_{\rm X}$ values against the mean photon arrival time per spectrum (Fig. 3), we find that an increasing or decreasing spectral slope is not a significant improvement over a constant value fit. The best-fitting constant value is $\beta_{\rm X} = 0.86 \pm 0.01$, while the standard error between the fit and the data points of 0.1 gives a measure of the scatter among the slopes about the constant fit value.

We derived the count rate to flux conversion of 1 count s^{-1} = 4.1×10^{-11} erg cm^{-2} s^{-1} from the time-averaged spectrum of the XRT PC mode data from 0.5 d onwards (to coincide with the time range covered by our final light-curve fits described in the following section).

An estimate for the spectral index between optical *R* and X-rays (centred at 1.7 keV) after 0.5 d results in $\beta_{\rm OX} \approx 0.65$. Note that this estimate does not take into account any optical extinction in the

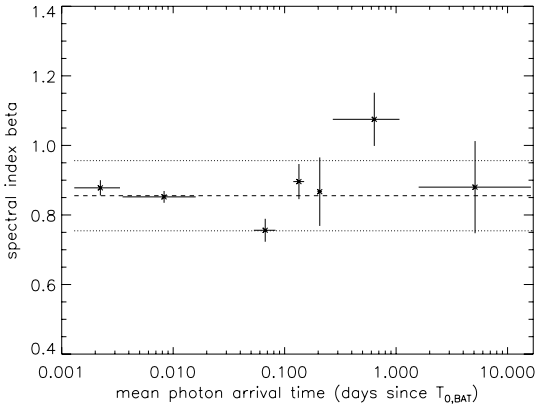

Figure 3. The X-ray power-law spectral index, β_X, as a function of the mean photon arrival time of the time-resolved spectra. The best-fitting constant value is overlaid (dashed line) together with the standard error between the fit and the data (dotted lines).

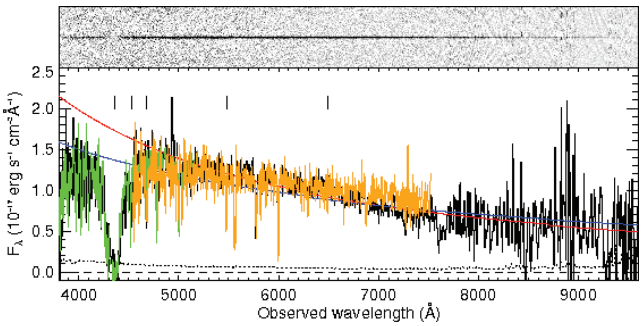

Figure 4. Optical spectra taken with the VLT, 0.7 d after the GRB event. The top panel shows the skyline-subtracted 2D spectrum from the 300V grism. The main panel shows the 300V (black), 1200B (green) and 600V (orange) 1D flux-calibrated spectra and the 300V error spectrum (dotted line). The H I Lyα and Si II lines used in metallicity determination are indicated above. The solid lines overplotted show power-law fits for the cases of $\beta_O = \beta_X$ (blue) and $\beta_O = \beta_X - 0.5$ (red), not including any host galaxy extinction.

host: we feel that our late-time optical data suffer from too much noise to reliably estimate any extinction in the host galaxy, while the assumption of a standard fireball model may not be valid at the time of the (early) UVOT data where extinction may be best measured. We also attempt to estimate the optical spectral index β_O using our optical spectra taken 0.7 d after the GRB event. The three spectra taken with the VLT are shown in Fig. 4. We overlay on these a power law with a spectral slope equal to that found in the X-rays ($\beta = 0.86$) and a power law with a slope shallower by 0.5 ($\beta = 0.36$) and see that both may be accommodated when all three spectra are included. Again, intrinsic extinction is not included in these power-law models and would be impossible to disentangle from the underlying spectral slope in this case. Thus, we conclude that we cannot reliably estimate β_O.

4.2 Light-curve fits

To obtain an estimate of some of the blastwave parameters, we fit the light curves and compare the results with the spectral slope for the X-rays. The full optical and X-ray light curves are shown in Fig. 5. We can obtain a good fit to the X-ray light curve using a smoothly broken power law, as suggested by, for example, Beuermann et al. (1999; subsequently explored further in Granot & Sari 2002), which

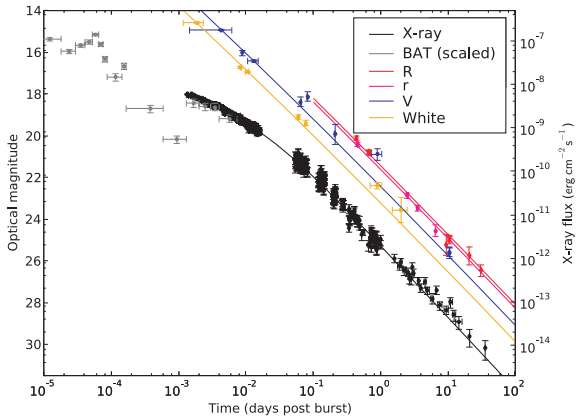

Figure 5. Gamma-ray (grey, BAT only), X-ray (black, final two points from *XMM–Newton*) and optical (colours: orange = white, blue = V and v, red/pink = R/r) light curves shown together. The solid lines show a smoothly broken power-law decay fitted to all bands from 430 s onwards (see Table 2). The optical magnitudes are corrected for Galactic extinction, while the X-ray fluxes are 0.3–10 keV observed fluxes. We have transformed the gamma-ray fluxes to the X-ray band using an absorbed power-law extrapolation.

allows for a smooth transition from one power law to another. We use the formulation

$$f(t) \propto t^{\alpha_2} \times \left(\frac{1 + (t/t_b)^{(s\cdot\gamma)}}{1 + (1/t_b)^{(s\cdot\gamma)}} \right)^{(-1/s)}, \quad (1)$$

with α_1 and α_2 are the decay parameters before and after the break, respectively, $\gamma = \alpha_2 - \alpha_1$, t_b the break time and s a 'smoothness' parameter for the break (fixed at the value of 1 throughout our fits). We omit the first 430 s of XRT data from the fitting, where we see deviations from a power-law shape (e.g. Marshall et al. 2008). Overlap between the XRT and BAT light curves at these very early times also suggests that the prompt emission may contribute significantly. Thereafter, the light curve decays in a very smooth fashion.

We simultaneously fit the optical data, where we keep the decay parameters for each optical band tied together. We initially employed models where the decay indices and break time of the X-ray light curve are free parameters, and the optical decays either as a smoothly broken power law (with the break time being the same as that in X-rays; Fig. 5) or as a single power law. The resulting difference between the latter two scenarios is minimal, but the preferred scenario is the smoothly broken power law for both the X-ray and the optical light curves, which improved the fits over a sharply broken power law fitted to the optical light curve (the F-test gives a probability of this result being obtained by a chance of 0.4 per cent). Based on these initial results, we see a difference at late times between optical and X-ray decay slopes of $\Delta\alpha \sim 0.25$, which is expected in one particular blastwave scenario (see the following section). We then fitted the models again, but this time we constrained the late-time light curves with a fixed 0.25 slope difference between the X-ray and the optical regime. The resultant fit parameters are shown in Table 2.

We then concentrate our efforts on the estimation of the light-curve decay of the very late-time data only, where we can be more confident that there is little to no influence of possible other components, including flares and energy injection. From 0.5 d onwards, we measure an X-ray decay of $\alpha_{X,2} \sim 1.4$ (Table 2). This is interestingly and significantly different from $\alpha_{X,2} \sim 1.6$ found when we fit the whole data set from 430 s onwards (in which a single break is best fitted at 0.02 d), and indicates a change in slope which

Table 2. Results of fits to the X-ray and optical light curves. sbpl = smoothly broken power law, pl = power law.

Model	$\alpha_{X,1}$	$\alpha_{X,2}$	$\alpha_{O,1}$	$\alpha_{O,2}$	t_{break} (d)	χ^2/d.o.f.
Data from 430 s						
$sbpl_X$, pl_O	$0.630^{+0.046}_{-0.049}$	$1.656^{+0.026}_{-0.025}$	1.272 ± 0.010	–	$0.0210^{+0.0039}_{-0.0032}$	508.4/411
$sbpl_X$, $sbpl_O$	0.630 ± 0.029	1.656 ± 0.015	$1.174^{+0.031}_{-0.025}$	$1.369^{+0.027}_{-0.031}$	$0.0210^{+0.0039}_{-0.0031}$	504.3/410
$sbpl_X$, pl_O with $\alpha_{X,2} = \alpha_O + 0.25$	$0.564^{+0.002}_{-0.010}$	$1.616^{+0.078}_{-0.164}$	1.366^a	–	0.0157 ± 0.0013	687.0/412
$sbpl_X$, $sbpl_O$ with $\alpha_{X,2} = \alpha_{O,2} + 0.25$	$0.630^{+0.005}_{-0.006}$	$1.656^{+0.019}_{-0.006}$	$1.153^{+0.019}_{-0.018}$	1.406^a	$0.0210^{+0.0023}_{-0.0029}$	506.2/411
Data from 0.5 d						
pl	–	$1.428^{+0.035}_{-0.034}$	–	$1.410^{+0.041}_{-0.039}$	–	55.3/58
pl, with $\alpha_{X,2} = \alpha_{O,2}$	–	$1.428^{+0.022}_{-0.035}$	–	1.428^1	–	55.6/59
pl, with $\alpha_{X,2} = \alpha_{O,2}$+0.25	–	$1.428^{+0.251}_{-0.011}$	–	1.178^1	–	98.7/59

[a]Constrained parameter, so the errors are taken from $\alpha_{X,2}$.

is not obvious when combined with earlier data. Fitting the optical and X-ray decay indices independently rather than being tied shows a difference of only 0.03, while any difference owing to a so-called cooling break (see the following section) between optical and X-rays should be $\Delta\alpha = 0.25$ in the fireball model (e.g. Sari et al. 1998). We thus conclude that there is no such spectral break in this scenario.

The question arises as to which of the two fits is actually better: the one containing data from 430 s onwards (smoothly broken power law) or the one with data only after 0.5 d (single power law). For this, we calculate the final χ^2 value, only for the data past 0.5 d, for both fits. That is, the fits themselves are still done by minimizing χ^2 calculated from the full applicable data range (post 430 s and post 0.5 d, respectively), but we compare χ^2 calculated by using only data past 0.5 d for each fit (where likely only a power law applies). The χ^2/d.o.f. for the smoothly broken power law in this case is rather bad, 111.1/55, compared to 55.3/58 for a power law only. This would indicate that the relatively good total χ^2 value for the smoothly broken power-law fit arises largely from the early data between 430 s and 0.5 d. This could be the case if errors in the early section are slightly overestimated. It could also indicate a second break at X-ray wavelengths in this interval, which would account for the difference in final power-law decays (α_X of 1.6 versus 1.4). Such a break would, however, increase the complexity of the underlying light-curve model and may make it more difficult to interpret the results. Lastly, we could also be seeing effects by fitting a smoothly broken power law, where the second decay index is the actual final decay index, and thus may not be equal to the decay index measured along a small portion of the light curve (see e.g. Jóhannesson, Björnsson & Gudmundsson 2006).

5 CONSISTENCY WITH THE FIREBALL MODEL

We now investigate whether or not the data are consistent with the fireball model predictions. We use the closure relations (found in e.g. table 1 of Zhang & Mészáros 2004) relating the optical and X-ray spectral and temporal slopes to determine how this GRB afterglow may fit into the standard fireball model. In Section 4.2, we have performed the same light-curve fits to two subsets of the data: one beginning at 430 s since the GRB and one beginning 0.5 d since the GRB, with two different outcomes. Following the reasoning in the last paragraph of Section 4.2, we examine the results obtained from fitting the data from 0.5 d to a single power law.

The late-time temporal fits show that the slopes are essentially the same in the X-ray and optical bands, with $\alpha \approx 1.40$, which indicates that both observing bands are in the same spectral regime, either both below or above the cooling break. In the case where they are both below the cooling break and the circumburst medium is homogeneous, the value of p can be derived to be 2.72 ± 0.20 from β_X (well within the range of previously found values; Shen, Kumar & Robinson 2006; Starling et al. 2008), and the predicted temporal slope is $\alpha = 1.29 \pm 0.15$, which is consistent with the observed value. A stellar-wind-like medium or a scenario in which both the optical and X-ray bands are situated above the cooling frequency can be ruled out by the standard closure relations between the spectral and temporal indices. The value for the X-ray spectral index, however, is somewhat at odds with the estimated β_{OX}, if there is no supposed break across the β_{OX} range. Host galaxy extinction may mean that the intrinsic optical magnitudes are brighter than those observed, allowing an increase in β_{OX}, which could resolve this apparent discrepancy. To investigate this, we can combine the *VRI* optical photometry (Table 1) with an X-ray spectrum to estimate extinction from the broad-band SED in the case that $\beta_O = \beta_X$. The SED, centred at 1.725 d, was created and fitted via the method outlined in Starling et al. (2007) and adopts a single absorbed power law as the underlying model and Small Magellanic Cloud-like host galaxy extinction. We find that extinction is required at the level of $E(B - V) = 0.21 \pm 0.07$, corresponding to $A_V \sim 0.6$ mag. This value is one of the highest measured for a GRB host galaxy (Starling et al. 2007; Schady et al. 2007a), but such measurements are made only for GRBs with detected optical afterglows and presumably extinction is much higher in the optically undetected dark bursts (e.g. Cenko et al. 2009; Fynbo et al. 2009).

For completeness, we performed the same tests on the best-fitting smoothly broken power-law model to the data from 430 s onwards. We find that the power-law index of the electron energy distribution, p, derived from the light curve predicts harder spectral indices than are observed. We investigated the possibility of an additional spectral component, caused by Inverse Compton (IC) emission, which would harden the spectrum (as also proposed for e.g. GRB 990123, Corsi et al. 2005, and GRB 000926, Harrison et al. 2001). Following the equations in Sari & Esin (2001) and Corsi et al. (2005), we find that the closure relations for the temporal and spectral indices still cannot be satisfied. We note that in this scenario, the break at 0.02 d may be considered an early jet break. There are two arguments against the attribution of this feature to the jet break. First, after a jet break the temporal slopes are given by $\alpha = p$, regardless

of whether the observing frequency is above or below the cooling frequency, so the optical and X-ray temporal slopes should be the same. This is not the case for this data set. Secondly, if this feature were a jet break it would imply an opening angle of 0°.44 (calculated using the equations in the following section), far smaller than most previously determined values (e.g. Frail et al. 2001; Berger, Kulkarni & Frail 2003, but see also Schady et al. 2007b; Racusin et al. 2008).

Concluding, the results from fits to the late-time-only data indicate that both observing bands are in the same spectral regime and in order to correctly predict the X-ray spectral slope the jet must be traversing a homogeneous medium. The difference between the optical-to-X-ray spectral index and the X-ray spectral slope is not predicted, but could be explained by the invocation of host galaxy extinction of $A_V \approx 0.6$. The results from using the full range of data cannot be satisfactorily described by the fireball model and/or with an early jet break, and it is likely that in this case a single smoothly broken power-law model is not applicable.

6 ENERGETICS

These data have shown that a late-time temporal break at X-ray or optical wavelengths is not required. We can therefore use the latest observation time as a lower limit to any jet break time and calculate the required limits on opening angle and total energy budget for the GRB jet. To calculate the isotropic energy $E_{\rm iso}$, we use the following equation:

$$E_{\rm iso}(\gamma) = \frac{4\pi \cdot S \cdot d_{\rm l}^2}{1+z}, \tag{2}$$

adopting the values listed in Sections 2 and 3 ($z = 2.591 \pm 0.001$, fluence $S = 8.81^{+0.77}_{-0.75} \times 10^{-5}$ erg cm^{-2}) and a luminosity distance $d_{\rm l}$ of 6.5×10^{28} cm (where $H_0 = 71$ km s^{-1} Mpc^{-1}, $\Omega_{\rm M} = 0.3$ and $\Omega_\Lambda = 0.7$, adopted in order to compare our value with the sample of Kocevski & Butler 2008). We find $E_{\rm iso} = 1.30^{+0.12}_{-0.11} \times 10^{54}$ erg. We have not included a K correction, because the energy range used encompasses the peak energy and the measured fluence should be sufficiently close to the bolometric fluence.[3]

Using this value for $E_{\rm iso}$, we can go on to calculate an upper limit on the jet opening angle (e.g. Frail et al. 2001), since no jet break is seen up to our last *XMM–Newton* observation. This is assuming we may apply the fireball model for the case of a uniform jet (see Section 5 for further discussion of this):

$$\theta_j = 0.057 \left(\frac{t_j}{1\,{\rm d}}\right)^{3/8} \left(\frac{1+z}{2}\right)^{-3/8} \left(\frac{E_{\rm iso}}{10^{53}\,{\rm erg}}\right)^{-1/8} \times \left(\frac{\eta_\gamma}{0.2}\right)^{1/8} \left(\frac{n}{0.1\,{\rm cm}^{-3}}\right)^{1/8}. \tag{3}$$

Adopting typical values for efficiency and density of $\eta_\gamma = 0.2$ and $n = 0.1$ cm^{-3}, respectively, we find $\theta_j \geq 0.127^{+0.002}_{-0.001}$ rad or $(7.30 \pm 0.08)^\circ$.

The lower limit on the total energy budget in gamma rays for the GRB is then obtained from the following equation which accounts for jet collimation using the newly derived jet opening angle upper limit:

$$E_\gamma = E_{\rm iso}(1 - \cos\theta_j), \tag{4}$$

which gives $E_\gamma \geq (1.06^{+0.07}_{-0.07}) \times 10^{52}$ erg, or more conservatively taking the lower limit for $E_{\rm iso}$, $E_\gamma \geq 9.88 \times 10^{51}$ erg using the end of the final *XMM–Newton* observation (36.08 d or 3.12×10^6 s) as our lower limit on any jet break time.

[3] For comparison, the rest-frame 1–10 000 keV fluence is $7.99^{+0.35}_{-0.36} \times 10^{-5}$ erg cm^{-2} corresponding to $E_{\rm iso,rest} = 1.18 \pm 0.05 \times 10^{54}$ erg.

7 DISCUSSION

7.1 Summary of results and associated caveats

We have followed the afterglow of the high $E_{\rm iso}$, relatively high-redshift GRB 080721 to beyond 10^6 s at both X-ray and optical wavelengths. The late-time decay is well fitted with a single power law with no requirement for a break. This suggests that the jet break must lie beyond the detection limits of the instruments used, and from this we calculate a lower limit to the total prompt gamma-ray energy of the GRB of $E_\gamma \geq 9.88 \times 10^{51}$ erg and to the jet opening angle of $\theta_j \geq 7^\circ.30$. This relies on the assumption that the fireball model describes the physics of the jet, that the jet is uniform in structure and that the standard values for the surrounding density and efficiency of energy conversion are applicable. We note that the dependence of the total energy on these latter two parameters is very weak (equation 2). We have compared the closure relations from the fireball model with the observed temporal and spectral slopes. The model and the observations cannot be reconciled for the whole data set, with departures from the model at early times (before half a day), and different temporal slopes are derived depending on whether data before 0.5 d are included in the fit. It is likely that additional components combine with the afterglow emission at the onset of the afterglow, rendering the fireball model inapplicable, but at what time the afterglow begins to dominate is not known. This illustrates the difficulties of pinning down the details of the blastwave physics even when broad-band well-sampled data are available. The data either from 0.5 d or from 430 s onwards require that the GRB jets traverse a homogeneous circumburst medium. The apparent inconsistency between the X-ray spectral index and the optical-to-X-ray spectral index may be caused by extinction in the host galaxy.

We have also investigated the alternative scenario in which an earlier break in the light curve at ~0.02 d is the jet break and found that this cannot work within the fireball model. If we assume the fireball model, and therefore that one of the measured observational parameters is contaminated (perhaps by an additional component or incorrect other assumption), then the implied jet opening angle would be very small (0°.44) for a GRB (or indeed any known jet source). Such collimation cannot be explained by any current models and the chances of the narrow jet happening upon our line of sight are small. We do not prefer this scenario for these reasons, but we note that this explanation has been the preferred model for some other GRBs which we discuss in Section 7.3. In the following subsection, we summarize the main classes of long GRB progenitor models and discuss whether any of these can reach energies 10^{52} erg and beyond.

7.2 Implications for gamma-ray burst progenitor models

In the collapsar scenario, two different ways to extract energy to make a GRB are suggested in the literature, one using neutrinos and the other harnessing magnetic fields.

In the neutrino-driven model, the energy that can be extracted depends sensitively on the accretion rate of collapsing material on to the newly formed black hole through the accretion disc and on the Kerr parameter describing the rotation of the black hole, as seen in table 3 of Popham et al. (1999; see also MacFadyen & Woosley 1999; Aloy et al. 2000; Nagataki et al. 2007). For typical long GRB durations (tens to hundreds of seconds), a GRB total

energy of 10^{52} erg is certainly possible within this model particularly for fast rotation rates. The observational testing of such models depends, therefore, not on measurements of GRB total energies but on determination of the rotation and mass accretion rates. According to the recent GRB progenitor models by Yoon & Langer (2005), Yoon, Langer & Norman (2006) and Woosley & Heger (2006), a lower metallicity star is preferred for a higher Kerr parameter. Yoon & Langer (2005) and Yoon et al. (2006) introduced models of chemically homogeneous evolution which produces helium stars with little or no hydrogen envelope that are metal-poor fast rotators, and can therefore go on to form a GRB. The complexities of stellar evolution are not all well understood and make the determination of GRB progenitors a difficult undertaking.

However, the identification of the crucial role of metallicity opens up an avenue for observational constraints. We can measure the metallicity of the circumburst medium or host galaxy along the line of sight to GRBs through afterglow spectroscopy, and for most long GRBs metallicities of the order of a tenth of the solar value have been inferred from this method (Fynbo et al. 2006; Prochaska et al. 2007), with the lowest measured value being $\frac{1}{100}$ solar for GRB 050730 (Chen et al. 2005; Starling et al. 2005b; Prochaska et al. 2007) though lines are often saturated hence likely to provide only lower limits on the metallicity (Prochaska 2006). We can measure the metallicity, Z, of the environment of GRB 080721 from the column densities of neutral hydrogen (H I Lyα) and singly ionized silicon (Si II λ1808 Å) in absorption (Fig. 4) of [Si/H] > -1.1. All the other observed spectral lines are likely to be saturated; hence, we have used the weakest detected metal line. This equates to $Z \sim 0.08$ times the solar value, within the typical distribution for GRBs. While this should strictly be treated as a lower limit due to possible saturation of the Si II λ1808 Å line, saturation is likely to be moderate at most and therefore the actual metallicity of the absorber should be of the order of one-tenth of solar, unless significant dust depletion effects are at play (as silicon is a mildly refractory element). If the metallicity is significantly lower than 0.1 solar, the Kerr parameter may be close to $a = 1$ (Yoon & Langer 2005; Yoon et al. 2006) and an energy of 1×10^{52} erg could be easily achieved according to the calculations of Popham et al. (1999). A high metallicity could be an indication of large initial stellar masses or simply that the models are not applicable.

The magnetic-field-driven model uses the Blandford–Znajek mechanism to extract rotation energy from the black hole (Blandford & Znajek 1977). This idea is indeed supported by the recent general relativistic magnetohydrodynamical simulations by Barkov & Komissarov (2008) and Komissarov et al. (2009). The energies that can be extracted are up to 10^{54} erg at 100 per cent efficiency. Typical efficiencies are likely to be far lower than this (but see Komissarov et al. 2009), and with 1 per cent efficiency the lower limit on the total energy of GRB 080721 can be accommodated. Here again the Kerr parameter is an important factor in determining the available energy, in which case lower metallicity progenitor stars may be preferable.

Interestingly, the measured energy limit for GRB 080721 is comparable to the energy budget in the magnetar scenario (Thompson, Chang & Quataert 2004), where the extraction of the rotational energy of a millisecond pulsar by strong magnetic fields is suggested (Duncan & Thompson 1992; Wheeler et al. 2000; Thompson et al. 2004; Komissarov & Barkov 2007). The magnetar scenario for long GRBs has received renewed interest in recent observational works, where it has been suggested to explain some plateau phases and very steep X-ray declines (Zhang & Mészáros 2001; Rosswog & Ramirez-Ruiz 2003, specifically in e.g. GRB 070110; Troja et al. 2007; Lyons et al. 2008). The claim of an 8 s periodicity in the highest energy bands for GRB 090709A suggests association with a magnetar for this source (Golenetskii et al. 2009; Gotz et al. 2009; Markwardt et al. 2009; Ohno et al. 2009). The theoretical prediction for the upper limit on the energy of a maximally rotating neutron star is few $\times 10^{52}$ erg (Thompson et al. 2004), and we note that $\sim 10^{52}$ erg is the lower limit we derive for this GRB implying very high efficiency close to 100 per cent. We therefore conclude that it is unlikely that GRB 080721 is produced via magnetar formation.

7.3 Comparison with other long gamma-ray bursts

The implied total energy for GRB 080721 based on the lower limit calculated here is not only a challenge to some progenitor models, but is a rare occurrence among GRBs. We have compared this limit to the energies measured from detections of jet breaks in a *Swift* sample of GRBs published by Kocevski & Butler (2008) in Fig. 6. The lower limit for GRB 080721 is much larger than any energy measured from a jet break in this sample. Comparing this source with the Amati relation (Amati et al. 2008) we see that it falls at the high $E_{\rm peak} - E_{\rm iso}$ end of the correlation, in a continuation of the long GRB population out to the most energetic sources. The *XMM–Newton* observations have enabled a longer baseline for jet searches and this source was chosen specifically for its unusually high isotropic energy.

GRB 061007 (Mundell et al. 2007; Schady et al. 2007b) was also a highly energetic GRB with an isotropic energy of 1×10^{54} erg (Golenetskii et al. 2006). The closure relations for this source were also not entirely satisfied and no spectral evolution was found from 80 s to 3.1 d after the trigger. The high implied total energy, in both the wind and homogeneous medium cases considered in Schady et al. (2007b), led the authors to conclude that an early jet break must have occurred, before T_0+80 s, which implies a highly collimated outflow with an opening angle of 0°.1–0°.8, four times smaller than any determined previously. This scenario, which we investigated for GRB 080721 in Section 5 and subsequently ruled out, requires that the narrow jet happens to lie along our line of sight, may be supported by the rarity of such non-evolving afterglows and the unusually high initial optical brightness for GRB 061007. However, we discussed long GRB progenitor models in the previous section for which the large energies measured both for GRB 061007 and in this paper for GRB 080721 when assuming a very late, unobserved jet break with a more typical jet opening angle are in fact achievable.

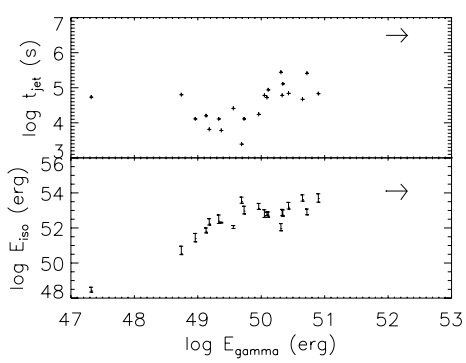

Figure 6. log E_γ – log $t_{\rm jet}$ (upper) and log E_γ – log $E_{\rm iso}$ (lower) plots for *Swift* long GRBs with jet breaks or possible jet breaks (taken from table 2 of Kocevski & Butler 2008; redshifts may be spectroscopic, photometric or from host association). The jet break time is given in the observer frame. The arrows in the upper right of each plot show the limits set here on GRB 080721.

Another case for which the observations implied a high-energy budget, while the standard fireball model was a poor description of the afterglow, was GRB 080319B (Racusin et al. 2008). This collapsar scenario for this long GRB is, however, supported by the detection of a supernova signature (Tanvir et al. 2008). To explain the complex afterglow behaviour, not smooth and featureless in this case but appearing to have a number of components including an initially extremely bright optical counterpart, Racusin et al. (2008) introduced a second jet. This two-jet model consisted of an inner jet with $t_{\rm jet} = 0.03$ d and an opening angle of $0\overset{\circ}{.}2$ and an outer jet more typical of GRBs with $t_{\rm jet} = 11.6$ d and an opening angle of 4°. Double and even triple jet systems are occasionally invoked when single jet models simply cannot explain the observations (e.g. GRB 030329, Berger et al. 2003; GRB 021004, Starling et al. 2005a; GRB 050401, Kamble et al. 2009; GRB 050802, Oates et al. 2007; De Pasquale et al. 2009), and while it is likely to be more physical to assume some structure across the jet (e.g. Rossi, Lazzati & Rees 2002; Zhang & Mészáros 2002), the interaction of multiple jets is not well known.

8 CONCLUSIONS

We have observed the bright, highly energetic afterglow of GRB 080721 out to 36 d since the trigger in the optical and X-ray bands. We conclude that no jet break is present in the late-time light curve and we rule out a jet-break origin for the early light-curve break, inferring a limit on the opening angle of $\theta_j \geq 7\overset{\circ}{.}30$ and setting constraints on the total energy budget of the burst of $E_\gamma \geq 9.88 \times 10^{51}$ erg within the fireball model. To obey the fireball model closure relations, the GRB jet must be expanding into a homogeneous medium and be extincted in the optical bands by approximately 0.6 mag. The energy constraint we derive can be used as an observational input for models of the progenitors of long GRBs. We can likely rule out a magnetar progenitor for this GRB as this would require close to 100 per cent efficiency to reach the observed total energy. Such high collimation-corrected energies could be accommodated with certain parameters of the standard massive star core-collapse models. One of the key observational parameters in distinguishing between various core-collapse models is the metallicity, diagnostic only if it lies outside of the typical range of $0.01 < Z < 0.1$. The metallicity we measure for GRB 080721 unfortunately does not allow a distinction between models to be made.

The occurrence of such highly energetic or narrowly beamed GRBs is rather rare, and for those which have the required measurements to allow a study such as this one on GRB 080721 we estimate that there may be a handful per year among the 100–130 well-localized GRBs currently triggering operational satellites. Measurement of the high-energy spectral peak, securing the redshift and monitoring the light curves for as long as possible (preferably in multiple bands) are all crucial, and these data have shown that a full understanding of the blastwave physics can be difficult to achieve even with a good quality, well-sampled, broad-band data set. To determine whether these sources are true outliers from the GRB population, perhaps requiring different or more extreme progenitors, will require dedicated efforts to build up small samples to compare with each other and with the growing data base of more typical GRBs.

ACKNOWLEDGMENTS

We acknowledge useful discussions with Andrew Read, Jenny Carter, Daniele Malesani and Tayyaba Zafar. RLCS, ER, KLP, KW, PAC and JPO acknowledge financial support from STFC. AJvdH is supported by an appointment to the NASA Postdoctoral Program at the MSFC, administered by ORAU through a contract with NASA. S-CY is supported by the DOE SciDAC Program (DOE DE-FC02-06ER41438). PJ acknowledges support by a Marie Curie European Re-Integration Grant within the 7th European Community Framework Program under contract number PERG03-GA-2008-226653, and a Grant of Excellence from the Icelandic Research Fund. This work made use of data supplied by the UK *Swift* Science Data Centre at the University of Leicester and *XMM–Newton* data taken under AO-7 Proposal No. 055597. The *Konus-Wind* experiment is supported by a Russian Space Agency contract and RFBR grant 09-02-00166a Based on observations made with ESO Telescopes at the Paranal Observatory under programme ID 081.D-0853. The INT and WHT are operated on the island of La Palma by the Isaac Newton Group in the Spanish Observatorio del Roque de los Muchachos of the Instituto de Astrofísica de Canarias. The LT is operated on the island of La Palma by Liverpool John Moores University in the Spanish Observatorio del Roque de los Muchachos of the Instituto de Astrofisica de Canarias with financial support from the UK Science and Technology Facilities Council. Based on observations made with the NOT, operated on the island of La Palma jointly by Denmark, Finland, Iceland, Norway and Sweden, in the Spanish Observatorio del Roque de los Muchachos of the Instituto de Astrofísica de Canarias. We thank Birgitta Nordstrom and Edita Stonkute for performing the NOT observations.

REFERENCES

Aloy M. A., Müller E., Ibáñez J. M., Martí J. M., MacFadyen A., 2000, ApJ, 531, L119
Amati L., Guidorzi C., Frontera F., Della Valle M., Finelli F., Landi R., Montanari E., 2008, MNRAS, 391, 577
Band D. et al., 1993, ApJ, 413, 281
Barkov M. V., Komissarov S. S., 2008, MNRAS, 385, L28
Berger E. et al., 2003, Nat, 426, 154
Berger E., Kulkarni S. R., Frail D. A., 2003, ApJ, 590, 379
Beuermann K. et al., 1999, A&A, 352, L26
Blandford R. D., Znajek R. L., 1977, MNRAS, 179, 433
Cenko S. B. et al., 2009, ApJ, 693, 1484
Chen H.-W., Prochaska J. X., Bloom J. S., Thompson B., 2005, ApJ, 634, L25
Corsi A. et al., 2005, A&A, 438, 829
Costa E. et al., 1997, Nat, 387, 783
Curran P. A., van der Horst A. J., Wijers R. A. M. J., 2008, MNRAS, 386, 859
D'Avanzo P. et al., 2008, GCN Circular 7997
De Pasquale M. et al., 2009, MNRAS, 392, 153
Duncan R. C., Thompson C., 1992, ApJ, 392, L9
Evans P. A. et al., 2007, A&A, 469, 379
Evans P. A. et al., 2009, MNRAS, 397, 1177
Frail D. A. et al., 2001, ApJ, 562, L55
Fynbo J. P. U. et al., 2006, A&A, 451, L47
Fynbo J. P. U. et al., 2009, ApJS, submitted (arXiv:0907.3449)
Galama T. et al., 1998, Nat, 395, 670
Golenetskii S., Aptekar R., Mazets E., Pal'shin V., Frederiks D., Cline T., 2006, GCN Circular 5722
Golenetskii S. et al., 2008, GCN Circular 7995
Golenetskii S. et al., 2009, GCN Circular 9647
Gotz D., Mereghetti S., von Kienlin A., Beck M., 2009, GCN Circular 9649
Granot J., Sari R., 2002, ApJ, 568, 820
Grupe D. et al., 2007, ApJ, 662, 443
Harrison F. A. et al., 2001, ApJ, 559, 123
Hjorth J. et al., 2003, Nat, 423, 847
Jakobsson P. et al., 2008, GCN Circular 7998

Jóhannesson G., Björnsson G., Gudmundsson E. H., 2006, ApJ, 640, L5
Kalberla P. M. W., Burton W. B., Hartmann D., Arnal E. M., Bajaja E., Morras R., Poppel W. G. L., 2005, A&A, 440, 775
Kamble A., Misra K., Bhattacharya D., Sagar R., 2009, MNRAS, 394, 214
Kocevski D., Butler N., 2008, ApJ, 680, 531
Komissarov S. S., Barkov M. V., 2007, MNRAS, 382, 1029
Komissarov S. S., Vlahakis N., Königl A., Barkov M. V., 2009, MNRAS, 394, 118
Kulkarni S. et al., 1999, Nat, 398, 389
Lyons N., O'Brien P. T., Zhang B., Willingale R., Troja E., Starling R. L. C., 2008, MNRAS, in press (arXiv:0908.3798)
MacFadyen A., Woosley S., 1999, ApJ, 524, 262
Markwardt C. B., Gavriil F. P., Palmer D. M., Baumgartner W. H., Barthelmy S. D., 2009, GCN Circular 9645
Marshall F. E., Guidorzi C., Ward P. A., Barthelmy S., Burrows D. N., Roming P., Gehrels N., 2008, GCN Report 156.1
Mészáros P., Rees M., 1997, ApJ, 476, 232
Mundell C. G. et al., 2007, ApJ, 660, 489
Nagataki S., Takahashi R., Mizuta A., Takiwaki T., 2007, ApJ, 659, 512
Nousek J. A. et al., 2006, ApJ, 642, 389
Oates S. R. et al., 2007, MNRAS, 380, 270
O'Brien P. T. et al., 2006, ApJ, 647, 1213
Ohno M. et al., 2009, GCN Circular 9653
Paczynski B., 1998, ApJ, 494, L45
Panaitescu A. et al., 2006, MNRAS, 366, 1357
Pian E. et al., 2006, Nat, 442, 1011
Popham R., Woosley S., Fryer C., 1999, ApJ, 518, 356
Prochaska J. X., 2006, ApJ, 650, 272
Prochaska J. X., Chen H.-W., Dessauges-Zavadsky M., Bloom J., 2007, ApJ, 666, 267
Racusin J. et al., 2008, Nat, 455, 183
Rhoads J., 1997, ApJ, 487, L1
Rossi E. M., Lazzati D., Rees M. J., 2002, MNRAS, 332, 945
Rosswog S., Ramirez-Ruiz E., 2003, in Fenimore E. E., Galassi M., eds, AIP Conf. Proc. Vol. 727, Gamma Ray Bursts: 30 Years of Discovery: Gamma-Ray Burst Symposium. Am. Inst. Phys., New York, p. 361
Sari R., Esin A. A., 2001, ApJ, 548, 787
Sari R. et al., 1998, ApJ, 497, L17
Schady P. et al., 2007a, MNRAS, 377, 273
Schady P. et al., 2007b, MNRAS, 380, 1041
Schlegel D. J., Finkbeiner D. P., Davis M., 1998, ApJ, 500, 525
Shen R.-F., Kumar P., Robinson E. L., 2006, MNRAS, 371, 1441
Stanek K. Z. et al., 2003, ApJ, 591, L17
Starling R. L. C., Wijers R. A. M. J., Hughes M. A., Tanvir N. R., Vreeswijk P. M., Rol E., Salamanca I., 2005a, MNRAS, 360, 305
Starling R. L. C. et al., 2005b, A&A, 442, L21
Starling R. L. C., Wijers R. A. M. J., Wiersema K., Rol E., Curran P. A., Kouveliotou C., Heemskerk M. H. M., 2007, ApJ, 661, 787
Starling R. L. C., van der Horst A. J., Rol E., Wijers R. A. M. J., Kouveliotou C., Wiersema K., Curran P. A., Weltevrede P., 2008, ApJ, 672, 433
Tanvir N. R. et al., 2008, ApJ, submitted (arXiv:0812.1217)
Thompson T. A., Chang P., Quataert E., 2004, ApJ, 611, 380
Tody D., 1986, Instrumentation in Astronomy VI; Proc. Meeting, Tucson, AZ. Part 2 (A87-36376 15-35). Society of Photo-Optical Instrumentation Engineers, Bellingham, WA, p. 733
Troja E. et al., 2007, ApJ, 665, 599
van Dokkum P. G., 2001, PASP, 113, 1420
van Paradijs J. et al., 1997, Nat, 386, 686
Wheeler C. J., Yi I., Höflich P., Wang L., 2000, ApJ, 537, 810
Willingale R. et al., 2007, ApJ, 662, 1093
Woosley S. E., Heger A., 2006, ApJ, 637, 914
Yoon S.-C., Langer N., 2005, A&A, 443, 643
Yoon S.-C., Langer N., Norman C., 2006, A&A, 460, 199
Zhang B., Mészáros P., 2001, ApJ, 552, L35
Zhang B., Mészáros P., 2002, ApJ, 571, 876
Zhang B., Mészáros P., 2004, Int. J. Modern Phys. A, 19, 2385

This paper has been typeset from a TEX/LATEX file prepared by the author.